Reconstitution de la variabilité climatique le long de la marge sud-chilienne (46°S) depuis le dernier maximum glaciaire

Calotte Nord Patagonienne
Photo : Jocelyn Chavy

Chapitre 4 – Reconstitution de la variabilité climatique le long de la marge sud-chilienne (46°S) depuis le dernier maximum glaciaire

Dans ce chapitre, j'ai reconstruit les changements climatiques qui ont affecté la marge sud-chilienne depuis la dernière période glaciaire en combinant la minéralogie des cortèges argileux, la géochimie élémentaire et la granulométrie afin de restituer la dynamique des glaciers, les changements dans le régime des précipitations et des vents d'ouest.

Les premières études sur les reconstructions paléo-climatiques en Patagonie se sont basées sur l'établissement d'une chronologie des avancées des glaciers andins (Caldénius, 1932) et sur les changements de végétations à partir de données polliniques (Auer, 1933). La reconstruction de la variabilité des calottes patagoniennes par l'identification des phases d'extension et de retraite des glaciers constitue une approche solide en climatologie car elles forment les plus larges réservoirs d'eau en dehors des régions polaires et sont extrêmement sensibles aux changements de température et aux alternances du régime de précipitations (Casassa *et al.*, 2000). Dans le contexte particulier qu'occupe la Patagonie, le climat est essentiellement contrôlé par l'intensité et la position de la cellule des vents dominants puisque l'Amérique du Sud est la seule masse continentale qui intercepte l'intégralité de la ceinture des Westerlies (SWW).

Les nombreuses études qui se sont développées dès lors se sont axées sur la variabilité dans la position et l'intensité de la SWW par l'utilisation d'indicateurs des précipitations et par les changements dans les températures des eaux de surface, en lien direct avec le courant circumpolaire Antarctique (Gilli *et al.*, 2005 ; Sepúlveda *et al.*, 2009 ; Tonello *et al.*, 2009 ; Waldmann *et al.*, 2009 ; Lamy *et al.*, 2010 ; Moreno *et al.*, 2010 ; Fletcher et Moreno, 2011). Cependant, en raison des forts gradients de précipitations nord-sud et ouest-est qui contrôlent la distribution de l'humidité sur le continent sud-américain, les signaux sont très souvent locaux car les indicateurs utilisés sont difficilement corrélables entre eux.

La multiplication des travaux sur les reconstructions paléo-environementales et paléo-climatiques se sont principalement focalisées sur les latitudes au nord de 41°S (Lamy *et al.*, 1998 ; 1999 ; 2001 ; Stuut *et al.*, 2007 ; Saukel *et al.*, 2011) et au sud de 51°S (Moy *et al.*, 2011 ; Schimpf *et al.*, 2011), laissant une large zone géographique (41 à 51°S) dépourvue d'archives climatiques.

De plus, les enregistrements collectés à ces latitudes sont souvent affectés par i) des contraintes temporelles imprécises et ii) des résolutions trop faibles pour observer une variabilité centennale à décennale.

Ce chapitre est donc divisé en deux parties rédigées sous la forme d'articles en préparation qui seront soumis après ma soutenance de thèse. Ces articles s'inscrivent dans la continuité d'une étude portant sur la variabilité de la minéralogie du cortège argileux et de sa signification paléoclimatique depuis la dernière période glaciaire dans la région d'Aisèn. Cette étude a été réalisée à plus faible résolution temporelle (Siani *et al.*, 2010 ; *Annexe 3*) et a montré que la minéralogie des argiles exprimée par le rapport Smectite/(Illite + Chlorite) et la géochimie élémentaire exprimée par le rapport Ti/K constituaient de bons indicateurs paléoclimatiques puisqu'ils permettent de retracer la variabilité des apports terrigènes.

Les résultats ont montré que la dernière période glaciaire (22 à 18 ka BP), caractérisée par des taux de sédimentation forts, est dominée par une érosion physique prononcée des roches ignées de la Chaîne côtière sous l'action intense des glaciers de la calotte nord patagonienne, en accord avec des conditions climatiques froides et arides au cours de cet intervalle. Néanmoins, cette période est également caractérisée par des variations à court terme illustrant des phases rapides d'avancées et de retraites des glaciers andins en réponse à la migration latitudinale à court terme de la cellule des vents dominants. Pendant la transition glaciaire/interglaciaire (18 à 11,5 ka BP), les données montrent un changement de contributeur dans la source des apports terrigènes avec une contribution croissante de l'altération des roches volcaniques de la Cordillère andéenne, excepté pendant l'intervalle de l'Antarctic Cold Reversal (14,4 à 12,2 ka BP). Enfin, l'Holocène est caractérisé par une dominance de la Cordillère andéenne probablement drainée par un système fluviatile plus développé et plus intense via les fjords, sauf pour quelques évènements sporadiques où la dynamique des glaciers va primer.

La publication en préparation intitulée : **« Highly detailed Holocene terrigenous sediment record and climatic variability along the Southern chilean margin : new insight on the northern Patagonian icefield fluctuations »** et qui sera prochainement soumise à *The Holocene*, a pour objectif la reconstruction de la variabilité climatique Holocène à partir des fluctuations de la fraction terrigène (minéralogie des argiles et granulométrie) le long de la marge sud-chilienne. Ces traceurs vont permettre d'expliquer les variations latitudinales de la cellule des vents d'ouest sur le continent et de leur éventuelle relation avec la dynamique des glaciers patagoniens (influence des précipitations sur le régime d'altération et/ou d'érosion des sources continentales et alimentation des glaciers). Un point fort de cette étude réside dans la robustesse du modèle d'âge employé pour dater l'enregistrement marin de la carotte MD07-3088 et par une résolution temporelle décennale à séculière de ces événements facilitant les corrélations avec les évènements climatiques historiques. Au début de l'Holocène, entre 11 et 9,7 ka , la récurrence d'événements marqués par la présence de grains grossiers (> 100 microns) dans la carotte MD07-3088 a été attribuée à une avancée de la calotte nord patagonienne. Ces résultats sont en accord avec ceux obtenus dans la région des fjords d'Aisèn par Harrison *et al.* (2012) traduisant une avancée des glaciers de la calotte nord patagonienne et à plus large échelle géographique par Putnam *et al.* (2012) qui a également montré une avancée des glaciers des Alpes Néo-zélandaises pendant le même intervalle de temps. La période de la Néoglaciation (7 à

3 ka) est aussi marquée par une considérable proportion de grains grossiers dans la carotte MD07-3088 témoignant d'une forte dynamique d'avancée des glaciers pendant cet intervalle de temps.

Enfin, à partir de ces résultats nous avons pu en déduire que les événements d'avancée des glaciers patagoniens au début de l'Holocène ne semblent pas être clairement liées à un forçage climatique régional exprimé en termes de variations de température et/ou de précipitations. En revanche, depuis l'Holocène moyen pendant la phase de Néoglaciation et jusqu'à l'actuel, les fortes précipitations traduiraient un lien direct avec l'avancée des glaciers patagoniens.

1. Highly detailed Holocene terrigenous sediment record and climatic variability along the southern chilean margin : new insight on the northern Patagonian ice-field fluctuations

Mélanie Carel, Giuseppe Siani, Christophe Colin, Guillaume Delpech

This paper will be submitted to ***The Holocene***

1. Introduction

Southern Patagonia presents outstanding conditions for paleoclimatic studies because mostly under the influence of the humid westerly winds and to its location in the windward side of the Andean cordillera, which lying athwart to the western air masses-driven moisture. In the last decades, many studies have been devoted to track the past Southern westerly winds (SWW) variability in the Southeastern Pacific area from continental and marine archives (Moreno et al., 2001; 2010; Lamy et al., 2001, 2004, 2010; Caniupán et al., 2011). Among these, some are no longer focused on the impact of the position and intensity of the Westerly winds on the coupled ocean-atmosphere system and their link with the atmospheric CO_2 orbital changes (Toggweiller et al., 2006; Waldmann et al., 2009; Moreno et al., 2010; Fletcher and Moreno, 2011; Varma et al., 2011). However, the exact timing and the latitudinal displacement of the westerly wind cells since the last glacial period still remains doubtful due to the lack of precise chronologies between marine and continental paleo-proxies.

At present time, the Patagonia region is partially recovered by two main icecaps, the northern and southern Patagonian icefields (NPI and SPI), which are the worldwide freshwater reservoir after Antarctica and Greenland respectively. It is widely assumed that these icefields are fueled by moisture transported from the Pacific Ocean via the westerlies winds inducing high rainfall throughout the year. High recorded precipitations are generated by the ocean-atmosphere control of the southern polar front that moves seasonally between 50°S (summer) and 40-45° (winter). Low-pressure anticyclones in the southern Pacific draw a great amount of moisture to the southern Chilean coast originating from the SWW marked by annual mean precipitations rate of ~ 3,000 mm (Fujiyoshi et al., 1987). The high elevation of the orogenic reliefs of the andean cordillera perturbs the distribution of the moist mid-latitudes westerly winds belt, inducing a strong west-east precipitation gradients (Warren and Sugden, 1993) underlying high rainfall rates on the western side of the Andes (Garreaud et al., 2009; Tonello et al., 2009).

Since the late glacial period, NPI and SPI glaciers underwent retreats and advances phases as showed by geomorphological and sedimentological studies as well as chronological dating on organic sediments or terminal moraines (Aniya, 1988, Aniya et al., 1997; Heusser et al., 2002; Glasser et al., 2004; Kaplan et al., 2005; Douglass et al., 2005; Boyd et al., 2008; Harrison et al., 2012). Moreover, most of these studies have been carried out on the eastern side of the Andes and many questions remain unanswered particularly with regard to the exact timing of the onset of the last deglaciation in the northern and southern Patagonian as well as at both sides of the Andean Cordillera (Mercer, 1982; Aniya and Sato, 1995; Douglass et al., 2005; Boyd et al., 2008; Harrison et al., 2012). Another unexplored point concerns the Northern Patagonia glacier variability during the Early to Middle Holocene, which was not previously recorded in the southern side (Harrison et al., 2012). Nevertheless, either the mechanism driving glacier fluctuations, or the nature and the exact timing of these events are still poor established.

The studied area is located along the south Chilean margin at approximately 46°S, offshore the region of Aysèn fjords between the northern Chonos archipelago and southern Taitao peninsula (Fig. 1). The area is a complex islands and channels landscape formed by extensive ice erosion from the North Patagonian icefield that covered this region during the last glaciation (Clapperton and Sugden, 1988) and it is present today at and near the mountain top of many of the higher altitudes extending over 4,200 km^2. The Aysèn fjords continuously receive freshwater mainly from the Aysèn river watershed and in minor contribution by marginal rivers like Rio Cisnés. Thirty outlet glaciers discharging from the North Patagonian icefield have been identified by Aniya (1988). Among them, two main glaciers from the northern part of the icefield flow to the west: glacier San Rafael, the lowest latitude tidewater glacier in the world and glacier San Quintin, the largest outlet from Northern Patagonian icefield that ends in a piedmont lobe.

Pioneer study focused on the reconstructions of SWW latitudinal shifts chronology at lower latitudes (33°S) using sedimentary proxies suggested that as well crystallinity and compostition of clay minerals and grain-size data of terrigenous sedimentary sequences could be used as powerful proxies to draw the continental weathering and thus by analogy to restore the rainfall intensity (Lamy et al., 1999). From then on, previous works of Siani et al., 2010, based on the study of the high sedimentation rate deep-sea core MD07-3088 collected offshore the Central Patagonian margin (46°S) suggested that is was equally possible to reconstruct the glaciers dynamic at higher latitudes, which is closely linked to precipitation rates continuously feeding glaciers, using clay assemblages parameters. Nevertheless, this solid hypothesis remains hard to demonstrate owing to the low temporal resolution. To lend further weight to this theory, here, we present the Holocene high-resolution terrigenous record through clay mineralogy and grain-size measurements from the deep-sea core MD07-3088. The close location of the studied core to the Northern Patagonian icefield and to the present-day maximum intensity of the southern westerly winds offers the opportunity i) to better constraining and providing new clues about the variability of the terrigenous supplies offshore the south-eastern chilean margin depending to westerly winds instability and ii) to establish a precise chronology of glaciers fluctuations of the Northern Patagonian icecap at high latitudes of the southern hemisphere during the Holocene. Otherwise, our record benefits of a very detailed chronological framework based on oxygen isotope analyses ($\delta^{18}O$) performed on the planktonic foraminifera *Globigerina bulloides* coupled to a large dataset of AMS ^{14}C dating of foraminifera and tephra markers (Carel et al., 2011; Siani et al., 2010, 2012).

2. Material and methods

2.1. Material

The Calypso core MD07-3088 was collected during the IMAGES PACHIDERME (MD159) cruise on February 2007 by the French R/V marion Dufresne in the South Pacific ocean off the Taitao peninsula (46`°04’30S; 75°41’23W; 1,536 m bsl; 18.9 m length; Fig. 1; Kissel, 2007). The core was

recovered on the continental slope where marine and alluvial and glacial continental deposits are layered from upstream marine terraces (Pinchemel, 1952).

The lithology of the core presents a fairly succession of olive black to greyish diatom and silt-bearing clay with some intercalations of silty-sandy layers (Fig. 2). In this study, the first 7 meters of the core are presented. The core MD07-3088 was sampled every 2 cm both for grain-size analyses and clay mineralogy. Careful sampling observation of sedimentary layers did not reveal imprints of turbiditic structures.

2.2. Methods

According to the isotopic stratigraphy previously defined by Siani et al., 2010, stable oxygen isotope ratio ($\delta^{18}O$), expressed in ‰ versus (Vienna Pee Dee Belemnite standard) was obtained on the planktonic foraminifera *Globigerina bulloides*. To improve the temporal resolution, sampling was refined every 5 cm. Six to ten shells were picked from the 250-315 μm size ranges. Prior to isotopic analyses, the samples were cleaned in a methanol ultrasonic bath during a few seconds then roasted under vacuum at 380°C for 45 minutes. Analyses were performed at LSCE (Laboratoire des Sciences du Climat et de l'Environnement, Gif sur Yvette) on Finnigan Delta+ mass spectrometer. VPDB is defined with respect to NSB19 calcite standard (Coplen, 1988). The mean external reproductibility (1σ) of carbonate standards is ± 0.06 ‰ for $\delta^{18}O$, measured NSB18 is -23.2 ± 0.2 ‰ VPDB.

Bulk sediments were treated successively with 0.1N hydrochloric acid (HCl) to remove carbonated fractions respectively. The mixtures were then rinsed several times to remove any residue of HCl.

Grain-size distribution measurements of particles in the range of 0.02 μm to 2,000 μm were carried out on a Malvern Mastersizer 2000 Particle Size Analyzer (affiliated with a "Hydro 2000G" sample dispersion unit) at the Laboratoire des Interactions et Dynamique des Environnements de Surface (IDES), Université Paris Sud. Ultrasonic oscillation was not used during the measurements as previous studies have shown that the use of ultrasonic dispersion could destroy the structure of some minerals (Boulay et al., 2003). In order to diminish errors, each sample was measured twice and the mean of the two measurements was employed to represent the grain-size distribution of the sample. In parallel, SEM images have been realized in the coarse fraction to observe morphologies of the particles. Several grains per each layer have been handpicked from the identified coarser layers in both fractions (> 40 μm and > 150 μm) and mounted on metal blocks. Pictures have been obtained under backscattered electrons on a Philips XL30 SEM (université Paris Sud).

X-Ray diffraction identification of clay minerals was conducted on oriented mounts of non-calcareous clay fraction (< 2 μm) by a PANalytical X'Pert Pro Diffractometer at the Laboratoire des Interactions et Dynamique des Environnements de Surface (IDES), Université paris Sud. The < 2 μm was previously separated by sedimentation according to the Stoke's law. The measurements were performed under three different conditions: air-dried, ethylene glycol-saturated and heated treatments.

Analyses under the air-dried and ethylene glycol-saturated conditions were performed for all the samples. One of every ten samples was chosen for measurements under heated conditions (500°C for 2 hours) to identify potential changes in the nature of clay minerals. The samples were X-rayed in the range of 3-30° 2θ with a step size of 0.03° 2θ and a measuring time of ~1second/step.

Proportions of different clay groups were calculated semi-quantitatively using peak areas of basal reflections for the main clay mineral groups on ethylene glycol-saturated samples using the MacDiff software (Petschick et al., 1996). Errors for calculation of percentage were estimated to about 2%. Relative proportions of kaolinite and chlorite were determined by ratios of areas of the (002) peak of kaolinite (3.57 Å) and the (004) peak of chlorite (3.54 Å). Relative proportions of different clay groups were given in percentages of the total clay assemblage.

3. Chronological framework

The stratigraphy of the core MD07-3088 was derived from the $\delta^{18}O$ variations of the planktic foraminifera *Globigerina bulloides*. As previously shown by Siani et al., 2010, $d^{18}O$ signature shows high variability throughout the Holocene. To improve $\delta^{18}O$ variability resolution, measurements were refined every 5 cm contrary to Siani et al., 2010 who presented $\delta^{18}O$ distribution every 10 cm.

The first part of the Holocene between 11.5 and 8 ka is characterized by mean lower $\delta^{18}O$ values that could reflect local hydrological changes marked by higher sea-surface temperature and/or lower salinity. However, despite these trends, short-term $\delta^{18}O$ large variability featured the entire Holocene period. The age model of the core was previously published in Siani et al. (2010) and Carel et al. (2011) and was based on nine AMS ^{14}C dates performed on monospecific planktonic foraminifera shells of *Globigerina bulloides* in the size fraction > 150 μm and one, concerning the top of the core, was done on epi-benthic foraminifera due to the very low concentration of planktonic forms. The conventional radiocarbon ages have been subsequently corrected using a regional reservoir age correction R_{surf} of approximately 800 years (Fig. 2; Siani et al., 2012). Then the ^{14}C ages have been calibrated using the calibration program Oxcal 3.10 with a 95% confidence level (2σ) (Bronk-Ramsey, 2009) based on INTCAL09 software (Reimer et al., 2004; 2009).

The average linear sedimentation rate is estimated at about 60 cm/ka during the last deglacial and Holocene. Taking into consideration the sampling interval (2 cm for grain-size and clay mineral and 5 cm for oxygen isotope analyses), we have obtained for the first time in the studied area an ultra-high temporal resolution of ca. 30 yrs for grain-size and clay mineral records and about 70 yrs for oxygen isotope record. In this study, hereafter, all ages will be discussed as calibrated ka BP.

4. Results

4.1. Clay mineral assemblages

Relative abundances of clay assemblage mineralogy are reported in Fig. 3. Throughout the sedimentary Holocene sequence, smectite, illite and chlorite are the dominant clay minerals, ranging from 20 to 60%, 15 to 40% and 15 to 35% respectively. Kaolinite is less abundant (not exceeding 5%) and exhibits a constant distribution pattern (Fig. 3). In general, illite and chlorite distributions are similar and inversely correlated to smectite.

Since the Early to Middle Holocene (11.5 to 7 ka BP), smectite content shows a continuous increasing trend from 25 to 50% whereas illite and chlorite decrease from 40 to 15% and 30 to 15% respectively. During the Middle to Upper Holocene, between ~7 to 1.4 ka BP, the trend is reversed with a diminishing content of smectite (60 to 20%) associated to an increasing of illite and chlorite (15 to 30% and 15 to 25%, respectively). Finally, between 1.4 to ~1 ka BP, smectite content follows again an increasingly distribution until 60% before starting over a descendant pattern, reaching minima of approximately 30% until present day. By contrast, illite and chlorite contents show opposite trends. The reduction of chlorite is more marked with a minimum of content of 15%, and an abrupt enrichment after 1 ka until 30% (Fig. 3).

Since, smectite and illite-chlorite have distinct temporal evolution and kaolinite does not present significant variations throughout the studied time interval, the smectite/(illite+chlorite), i.e. the S/(I+C) ratio was calculated to describe the mineralogical variations within the clay fraction (Fig. 3). This mineralogical ratio shows significant variations throughout the Holocene. The Early Holocene is characterized by low values of S/(I+C) ratio of about 0.5. The increasing trend until higher values of 2 explains stronger contribution of smectite in clay assemblages from about 11 to 7 cal. ka BP. During the Middle Holocene (7 to 3 cal. ka BP), S/(I+C) ratio lies on a decreasing trend displaying initial Early Holocene values (2 to 0.5). This decreasing distribution continues till the Upper Holocene since about 1.4 ka BP, when an abrupt short-term increase of the lasting ~ 0.4 ka BP is recorded. Finally a new S/(I+C) ratio decreasing trend was recorded until present-day (Fig. 2).

However, superimposed on the general increasing and decreasing trends of the clay mineral records, short-term centennial to millennial-scale fluctuations marked the whole Holocene period.

4.2. Siliciclastic grain-size

Relative standard deviation as a function of the grain-size classes reported in Fig. 4 show the dominance of three populations throughout the Holocene marked by a fine class estimated at the half height between 5 and 15 μm, a medium fraction between 30 and 100 μm and a coarser fraction > 100 μm. In the Fig. 5 are reported the distributions of these three dominant fractions as a function of time. Sediment grain-size is largely dominated by fine particles (5 to 15 μm) that represent 30 to 50% of the total sediment followed by medium size particles (30-100 μm) from 20 to 45% and finally by coarse size particles (> 100 μm) reaching maxima of 5% for individual layers. Interestingly, largest variations are observed in the proportion of the > 100 μm fraction which evidences the presence of coarser layers over the last 12 ka BP in agreement with the distribution of the mean grain-size variability (from 15 to

30 %), and which are not correlated with previously recognized tephra layers (Fig. 5; Carel et al., 2011). During the Early to Middle Holocene (11.5 to 7 ka BP), coarser layers are identified by 3 main episodes, between 11.6 ka BP to 9.0 ka BP and two lesser episodes at 8.4 ka BP and between 7.3 and 6.9 ka BP respectively. The first part of the Middle Holocene (7 to 5 ka BP) is characterized by a higher short-term frequency of coarser layers closely spaced in time and punctuated by 5 episodes centred between 7 to 5.0 ka BP (Fig 6). By contrast, a slightly decreased frequency of coarser layers marks the interval between 5.0 to 3.0 ka BP with three major events centred at 4.0, 3.7 and 3.2 ka BP respectively. Finally, the Upper Holocene (3 ka to present day) is illustrated by two lesser distinct events at 2.9 ka BP and between 2.1 and 1.4 ka BP (Fig. 6).

4.3. Morphoscopy and mineralogy of coarser layers

SEM geochemistry and imaging obtained on several detrital particles counted in the > 150 μm fraction in all coarser layers reveals that quartz is the most abundant mineral in the terrigenous fraction, followed by K-rich feldspars. Morphoscopic analyses realized on the quartz grains show typical sub-rounded, fractured and blunted shapes probably resulting from shock due to intense transport dynamic (Fig. 5). Such specific criteria show that terrigenous particles are probably the result of turbulent fluviatile flow associated to glacier mass movement (Haritashia et al., 2010).

5. Discussion

Mineralogy and grain-size of the terrigenous fraction are exclusively controlled by three main factors: (1) the nature of the continental eroded source, (2) the intensity and mode of the continental weathering and (3) the vector of transport which drains detrital inputs (Nesbitt and Young, 1996). Then, results will be discussed in term of glacier Holocene variability in this region and at wider hemispheric scale in order to restore the causes and mechanisms of such changes.

5.1. Mineralogical discrimination of particles provenance

Under the low hydrolysis conditions characterizing the high latitudes of the southern Chile, mineralogical composition could be related to a modification of the sedimentary sources, strongly influenced by climate changes (Chamley, 1989). As previously shown by Siani et al., 2010, two main potential sources can be distinguished. The geology of the studied region is characterized by two main physiographic units. The main geological formations of the Coastal Range consist of primarily pre-Jurassic low-grade metamorphic basement, intermediate igneous rocks and ophiolites (Zeil, 1986). Farther east, the lower part of the Andean cordillera is constituted by 3,000 m high Mesozoic intermediate calc-alkaline plutonic rocks (Patagonian Batholith), whereas volcanic arc itself is composed by pre-Pliocene andesitic ignimbrites overlain by Plio-Quaternary volcanics and tephras

resulting from different explosive events of the main subduction-related Cenozoic volcanic centres (Cay, Maca and Hudson volcanoes, Forsythe et al., 1986; Zeil, 1986; Stern, 1996).

On one hand, illite and chlorite are primarily minerals concentrated in the igneous formations. Illite and chlorite derive from the alteration of primary minerals like muscovite and biotite from the low-grade metamorphic and plutonic rocks constituting the Coastal Range and the lower parts of the Andes forming the Patagonian Batholith (Niemeyer et al., 1984; Fig. 1). On the other hand, smectite derives mainly from weak (or moderate) chemical weathering of Ti and Fe-rich volcanic and volcanoclastic rocks forming the high reliefs of the Andean cordillera (Forsythe et al., 1986; Fig. 1). Furthermore, smectite could also result from hydrolysis of primary minerals associated to the alteration of bisialitic soils (Colin et al., 2001), which are, in turn, poorly developed in the high latitudes Chilean region. From these observations, we can consider only the volcanic source at the origin of smectite contents as already stated by Siani et al. (2010).

Kaolinite could be attributed to highly weathering of lateritic soils, which take place essentially in tropical and sub-tropical environments (Chamley, 1989). However, taking into account the geological and climatic context of the studied area, we deduce that the low kaolinite content could likely originate from the physical erosion of sparse sedimentary sequences from the Coastal Range.

Prevailing low values of the S/(I+C) ratio at the last deglacial/Holocene transition suggest a dominance of Coastal Range erosion supplies. Marked changes in the continental source, as displayed by an increase of the smectite content, characterize the Early to Middle Holocene (11.5 to 7 ka BP) suggesting a major imprint of terrigenous material originating from the weathering of the Andes (Fig. 3). An outstanding opposite trend of the S/(I+C) ratio is recorded during the Middle to Upper Holocene between ~ 7 to 1.5 ka BP, pointing out the influence of the Coastal Range inputs marked by higher contents of illite.

It should be emphasized that the high-resolution clay mineralogy composition recorded in this study shows that the origin of detrital particles is often a mixture between various rocks sources from granitoidic and low-grade metamorphic bedrock and volcanic components of highest Andean chain. This could be induced by short-term climate changes in the study area affecting the intensity and the origin of the erosive processes. Indeed, though the S/(I+C) ratio clearly show general increasing (11.5 to 7 ka BP) and decreasing (7 to 1.5 ka BP) trends across the entire Holocene, pronounced short-term amplitude changes featured this period. About this point, Bertrand et al. (2012) recently suggested that changes in drainage areas, volcanic activity and glacier cover could vary considerably along the Holocene period in the Taitao and Aisèn fjords region and consequently may have affected the terrigenous provenance and supply.

5.2. Transport dynamic

Grain-size results provide some constraints about the dynamic of transport of sediments. Grain-size pattern evidenced peculiar outlines during the Holocene in agreement with the previously

determined mineralogical signature variations (Siani et al., 2010). Several coarser layers mark the Early Holocene between 11.6 and 9.0 ka BP (Fig. 4) indicating a more proximal contribution from the neighbouring Coastal Range erosion. Associated to increasing smectite influence, finer silty particles dominate the Early Holocene suggesting more distal inputs from Andean chain located farther east compared with the position of the marine core (Fig. 1). The Middle Holocene events, illustrated by abundant coarser particles, are most likely the results of proximal environments dismantling remains of Coastal Range in accordance with higher contents of illite and chlorite.

North-south transects along the Chilean margin reveal the influence of at least 4 modes of transport influenced by rainfall variability: aeolian, current-derived material, fluviatile and glacial via the deep fjords (Stuut et al., 2007). In the northernmost part, aeolian transport prevails due to arid climatic conditions (Potter, 1994), whereas between 33 and 44°S, Mediterranean-type climate favours more important precipitations causing a more intense fluvial transport with the development of denser drainage areas. Heavy rainfalls south of 44°S explain the alternation with fluvial and glacial bedload with important coarser debris during glacial times due to the presence of the two active continental Patagonian icefields (Glasser et al., 2004; Kaplan et al., 2005). Because of the direction of the prevailing westerly belt, silty and sandy supplies couldn't be originated neither from aeolian dust transport, in accordance to the high mean value of the terrigenous flux (~130 $g.cm^{-2}.ka^{-1}$) or derived from currents which are not sufficiently intense nearby the coast (Stuut et al., 2007). Furthermore, the weak balance of sea level throughout the Holocene (from -35 m to 0 m) excludes potential supplies from northernmost or southernmost locus.

In addition, the position of the core MD07-3088 offshore the Aisèn fjords region explains the dominance of inputs either from both fluviatile networks and glacial valleys. Nevertheless, it is possible to distinguish fluviatile inputs and/or glacial supplies by the presence of coarser layers throughout the Holocene directly dependent on the high sedimentation rates (~60 cm/ka). Coarse layers contain large amounts of sandy-size particles (> 100 μm) whose origin could not be attributed to fluvial runoff. Proglacial river sediments are mostly dominated by typically silty particles (between 6 and 20 μm) as suggested by Haritashia et al. (2010). However, the distance between our coring site and river mouths is too consequent to supply highly coarser material. Glacier studies focalised on Neoglacial glaciers fluctuations at 46°S evidenced the proximal behaviour of the coarse fraction suggesting that sandy particles mostly result from fjords dynamic via glacier ablation whereas finer material (clayey and silty) result from fluviatile runoff activity (Bertrand et al., 2011). We can thus consider the occurrence of coarser layers as a direct response of an intense glaciers bedload. Particles shape and associated diameter, determined on characteristic coarser layers, are reported in Fig. 5 and evidence a combined transport by proglacial rivers and glaciers. Indeed, grain-size is dominated by two main classes centred at 40 and 400 μm.

5.3. Comparison with Holocene glacier fluctuations chronology

The robust chronological framework established for the core MD07-3088 represents a solid starting point to provide new insight about the exact timing of the Holocene glacier evolution in the central Patagonia thus facilitating comparison with other climatic records at regional and global scale. The Early Holocene is characterized in our record by two major coarser events recorded between 11.6 and 11.4 ka BP and 10.0 and 9.0 ka BP respectively (Fig. 6). These events are coeval, within age uncertainties at 2σ, with previous published glacier advances recorded east of the Andes in Rio Bayo Valley, the major outlet of the northernmost North Patagonian Icecap glacier Exploradores (Glasser et al., 2006). The authors, by using OSL (single-grain optically stimulated luminescence) and cosmogenic nuclide surface exposure dating indicated glacier advances at ca. 10.9 ± 1 and 9.7 ± 0.7 ka BP respectively. Evidence of a synchronous glacier advance between 10.7 to 10.5 ka BP was done by geomorphological reconstructions coupled to radiocarbon dating of organic sediment within terminal moraine at Lake Elizalde located in the nearby Aisén region (Mardones et al., 2011). More recently, a coeval glacier advance was also reported west of the Andes by OSL dating at Tempanos moraine (laguna San Rafael, 46°S) dated between 9.3 ± 1.2 and 9.7 ± 1.2 ka BP (Harrison et al., 2012).

During the Early to Middle Holocene, two coarser event was recovered in core MD07-3088 at 8.4 ka BP and between 7.3 and 6.9 ka BP. This was previously evidenced by glacier advances dated at 8.5 ± 0.7 ka BP by cosmogenic isotopes in three moraines at Fachinal along the eastern flanks of the Patagonian Andes (Douglass et al., 2005) and at Laguna San Rafael by OSL dating at ca. 7.7 ± 1 ka BP (Harrison et al., 2012).

The major recurrence of coarser events was however recorded in core MD07-3088 during the Middle Holocene between 7 to 3 ka BP. This time interval is related to the settlement of cooler conditions in the Southern Hemisphere, corresponding to the Neoglaciation period (Mercer, 1970; Denton and Karlen, 1973). At least five major coarser events split up into the Middle Holocene. The first centred between 5.8 and 5.2 ka BP marked by three closely spaced in time events, whereas the remaining were recovered at 5.0 ka BP, 4.0 ka BP and at 3.7 ka BP respectively. Glacier advance dated at 6.2 ± 0.8 ka BP and at 5.7 ± 0.6 ka BP have been recorded by cosmogenic dating at Facinal (Douglass et al., 2005) and at San Rafael outlet glaciers by OSL dating (Harrison et al., 2012) respectively. The following major coarser events recorded in core MD07-3088 between 4.0 and 3.2 ka BP is in excellent agreement to an advance of Gualas glacier between ~ 4.2 and 3.2 ka BP as recorded by the sedimentary sequence in the nearby fjord of Golfo Elefantes (Bertrand et al., 2012). Similarly, during the Upper Holocene a major coarser event dated at ~ 2.9 ka BP followed by silty-sandy events dated between 2.1 to 1.4 ka BP in our record are coeval to a major Gualas glacier advance dated between 2.9 to 2.1 ka BP (Bertrand et al., 2012) and also recorded in Quetro river valley in the Aisèn region (Mardones et al., 2011).

At wider regional scale, the sedimentary record of core MD07-3088 versus NPI glacier variability is in general good agreement with “Mercer-type” and “Aniya-type” chronology from the SPI outlet glaciers covering the last 5 ka BP (Mercer, 1970; Aniya and Sato, 1995; Fig. 6). However, it should be noted that no glacier advances were recorded along the SPI during the Early Holocene.

During the Middle to Upper Holocene the 4.0 to 3.7 and 3.2 ka BP events are coeval to "Mercer-type" and "Aniya-type" chronologies that includes a maximal glacier advance between 4.7 to 4 ka BP and 3.6 ka BP respectively according to the Neoglacial advance I. The 2.9 ka BP event can be related, within age uncertainties at 2s, to the combined Mercer and Aniya chronologies, which evidenced extension maxima between 2.0 to 2.7 ka BP that corresponds to the Neoglacial advance II.

5.4. Relationship with Holocene climatic changes

Glacier fluctuations are commonly attributed to important climatic conditions changes. At a global scale, Holocene glaciers variations are directly dependent on three main forcing factors: i) temperature and related ablation, ii) precipitations and rain-fuelled snow accumulation and iii) internal ice dynamic not climatically driven (Warren and Sugden, 1993; Anderson et al., 2010). To better interpret Holocene icecap fluctuations and decipher the control of temperature and/or precipitations control, our multi-proxies terrigenous record is compared with palynological and summer sea-surface temperatures reconstructions obtained in the same record (46°S; Montade et al., 2012; Siani et al., 2012; Fig. 7) and with sea-surface temperatures recorded in the northernmost Lago Condorito record (41°S; Moreno et al., 2010; Fig. 7) and southernmost Tamar Lake (52°S; Lamy et al., 2010; Fig. 7). Palynological studies are based on the variability of the concentration of *Nothofagus-type* pollen, which behaviour is closely linked to annual precipitations (Tonello et al., 2009).

During Early to Middle Holocene, identified glacier advances are coeval with low values of *Nothofagus dombeyi* at 46°S, even though a slight and progressive expansion is recorded between 12 and 7 ka BP. Associated to the increase of heliophytic trees and expansion of *Myrtaceae*- and *Tepualia*-type vegetations (Montade et al., 2012), this time interval is characterized by relatively low precipitations. Moreover, summer SST reconstructions in the core MD07-3088 display relatively uniform values (~2°C), suggesting low temperature variations. These findings match with a southward position of the Southern Westerlies centred between 50 and 55°S during the Early Holocene (Lamy et al., 2010), in agreement with the higher precipitations recorded southernmost in Tamar Lake (52°S; Lamy et al., 2010) whereas the northernmost area of Lago Condorito (41°S) is subjected to a weaker pluviometry (Moreno et al., 2010). Warmer and drier conditions that seems to prevail during Early Holocene cannot explain glacier advances during this time span, which could respond to the internal ice dynamic transition between calving and not calving phases as previously suggested by Harrison et al. (2012) to explain Early Holocene glacier advances recorded in nearby Laguna San Rafael. Nevertheless, sensitive temperature variations (~1°C) must be taken into account because at wider scale, glacier advances in Southern Alps (New Zealand) have been recorded at 10.7 ± 0.4 ka BP and 9.8 ± 0.4 ka BP by ^{10}Be surface-exposure method, coeval with our record and explained as a result of a 1°C temperature variation (Putnam et al., 2012).

The 7 to 3 ka BP interval (Neoglaciation phase) is marked by a strong recurrence of short-term advance events evidenced by grain-size, correlated to increasing precipitation and thus more snow

accumulation at 46°S (Montade et al., 2012) as equally shown by chiromids record (Massafero and Brooks, 2002). Wetter conditions are associated to low sea-surface temperatures (~2°C) suggesting a northward migration and strengthening of the winds cell, in agreement with the maxima of rainfall recorded in Lago Condorito (41°S; Moreno et al., 2010) and decreasing precipitations in southernmost (52°S; Lamy et al., 2010).

The Upper Holocene (the last 3 ka BP) is marked by relatively steady high concentrations of *Nothofagus dombeyi* at 46°S even though a decrease is recorded both northernmost (41°S) and southernmost (52°S) suggesting a return of Westerlies winds cell to its initial position but slightly north of 50-55°S.

6. Conclusion

In this study, we present a high-resolution clay mineralogy and grain-size record to restore continental climate variability from a marine record recovered off the southern Aisén fjords region by interpretation of continental source supplies and glaciers dynamic giving precious information about latitudinal shifts of Westerly winds belt since the last 12 ka BP.

Results show important changes in the contribution of the source rocks, from distal volcanics of Andean cordillera during the Early Holocene (12 to 7 ka BP) to proximal plutonic rocks and low-grade metamorphic basement of the Coastal Range during Middle and Late Holocene (7 ka BP to present) evidenced by higher variability of the smectite/(illite + chlorite) ratio. These findings are supported by evidences of coarser layers, which recurrence is directly associated to the Northern icecap fluctuations.

The Early Holocene (12 to 7 ka BP) detrital supplies are illustrated by enhanced chemical weathering of the volcanic rocks of the high reliefs of the Andean cordillera, mainly driven by fluviatile vector. However, this time interval is punctuated by several evidences of glaciers activity dated between 11.6 and 11.4, 10.0 and 9.0, at 8.4 and between 7.3 and 6.9 ka BP, suggesting colder and wetter conditions, intensified rainfall and snow accumulation reflecting northward migration of the SWW. At the opposite, the Middle Holocene time span is illustrated by dominance of illite and chlorite in clay assemblage and higher proportion of coarser layers implying the contribution of the proximal Coastal Range and glaciers dynamic as the main driver of the terrigenous inputs. Evidences of glacial advances are recorded at higher short-term frequency between 7 and 5.0 ka BP concordant with the Neoglacial phase in southern hemisphere, before starting a slightly decreasing in frequency between 5 and 3 ka BP. Cooler and wetter conditions recorded during Middle Holocene are the direct consequence of the northward migration of the SWW, favouring intense snow accumulation over the growing Northern Patagonian icecap.

Finally, Late Holocene (3 ka BP to present) shows a higher short-term fluctuations, from climatic conditions similar to those of the Early Holocene between 3 and 1.4 ka BP, with minor coarser events and slightly increasing trend of smectite, whereas conditions similar to those of Neoglacial interval are

recorded after, with smectite starting to decrease after 1.4 ka BP. It seems to agree with the return to colder conditions induced by a slightly northernmost position of the SWW compared to modern position.

Acknowledgments

This study has been realized within the framework of the international IMAGES program and the MD159 PACHIDERME cruise that authors gratefully acknowledged. Thanks are also addressed to the crew of R/V Marion Dufresne. We thank C. Moreau and J.-P. Dumoulin and ARTEMIS group for the acquisition of AMS radiocarbon dating. R. Pichon is equally thanked for his precious help in SEM imaging. C. Kissel, E. Michel and G. Isguder are acknowledged for useful discussions.

References

Anderson, M.L., Larsen, T.B., Nettles, M., Elosegui, P., van As, D., Hamilton, G.S., Stearns, L.A., Davis, J.L., Ahlstrøm, A.P., de Juan, J., Ekström, G., Stenseng, L., Khan, S.A., Forsberg, R., Dahl-Jensen, D., 2010. Spatial and temporal melt variability at Helheim Glacier, East Greenland, and its effect on ice dynamics. *Journal of Geophysical Research*, vol. 115, pp. 18.

Aniya, M., Naruse, R., Casassa, G., Rivera, A., 1997. Variations of Patagonian glaciers, South America, utilizing RADARSAT images. *Proceedings of the International Symposium on RADARSAT Application Development and Research Opportunity (ADRO)*, Montreal, Canada, 13–15.

Aniya, M., Sato, H., 1995. Holocene glacial chronology of Upsala Glacier at Peninsula Herminita, Southern Patagonia Icefield. Glacier research in Patagonia. *Bulletin of Glacier Research* 13, 83–96.

Aniya, M., 1988. Glacier inventory for the Northern Patagonia Icefield, Chile, and variations 1944/45 to 1985/86, *Arctic and Alpine Research* 20, 179–87.

Bertrand S., Hughen K.A., Lamy F., Stuut J.B.W., Torréjon F., Lange C.B., 2011, Precipitation as the main driver of Neoglacial fluctuations of Gualas glacier, Northern Patagonian Icefield. *Climate of the Past Discuss*ions 7, 2937–2980.

Bertrand, S., Hughen, K.A., Sepúlveda, J., Pantoja, S., 2012. Geochemistry of surface sediments from the fjords of Northern Chilean Patagonia (44–47°S) : Spatial variability and implications for paleoclimate reconstructions. *Geochimica et Cosmochimica Acta* 76, 125–146.

Boulay, S., Colin, C., Trentesaux, A., Pluquet, F., Bertaux, J., Blamart, D., Buehring, C., Wang, P., 2003. Mineralogy and sedimentology of Pleistocene sediment in the South China sea (ODP site 1144). *Proceedings of the Ocean Drilling Program, Scientific Results*, vol. 184, pp. 21.

Boyd, B.L., Anderson, J.B., Wellner, J.S., Fernandez, R., 2008. The sedimentary record of glacial

retreat, Marinelli fjord, Patagonia: Regional correlations and climate ties. *Marine Geology* 255, 165 – 178.

Bronk-Ramsey, C., 2009. Bayesian analysis of radiocarbon dates. *Radiocarbon* 51, 337–360.

Caniupan, M., Lamy, F., Lange, C.B., Kaiser, J., Arz, H., Kilian, R., Baeza Urrea, O., Aracena, C., Hebbeln, D., Kissel, C., Laj, C., Mollenhauer, G., Tiedemann, R., 2011. Millennial-scale sea surface temperature and Patagonian Ice Sheet changes off southernmost Chile (53°S) over the past ~60 kyr. *Paleoceanography* 26, PA3221, 1–10.

Carel, M., Siani, G., Delpech, G., 2011. Tephrostratigraphy of a deep-sea sediment sequence off the south Chilean margin : New insight into the Hudson volcanic activity since the last glacial period. *Journal of Volcanology and geothermal Research* 208, 99–111.

Chamley, H., 1989. Clay Sedimentology. *Springer*, Berlin, 623 pp.

Clapperton, C.M., Sudgen, D.E., 1988. Holocene glacier fluctuations in South America and Antarctica. *Quaternary Science Reviews*, vol. 7, 185–198.

Colin, C., Bertaux, J., Turpin, L., Kissel, C., 2001. Dynamique de l'érosion dans le bassin versant de l'Irrawaddy au cours des deux derniers cycles climatiques. Comptes Rendus de l'Académie des Sciences – Séries IIA – *Earth and planetary Science*, vol. 332, issue 8, 483 – 489.

Coplen, T.B., 1988. Normalization of oxygen and hydrogen isotope data. *Chemical Geology* 72, 293–297.

Denton, G.H., Karlen, W., 1973. Holocene climatic variations ; their pattern and possible cause. *Quaternary Research* 3, 155–205.

Douglass, D.C., Singer, B.S., Kaplan, M.R., Ackert, R.P., Mickelson, D.M., Caffee, M.W., 2005. Evidence of early Holocene glacial advances in southern South America from cosmogenic surface-exposure dating. *Geology*, vol. 33, no. 3, 237–240.

Fletcher, M.S., Moreno, P.I., 2011. Zonally symmetric changes in the strength and position of the Southern Westerlies drove atmospheric CO 2 variations over the past 14 k.y. *Geology* 39, 419–422.

Forsythe, R.D., Nelson, E.P., Carr, M.J., Kaeding, M.E., Hervé, M., Mpodozis, C.M., Soffia, M.J., Harambour, S., 1986. Pliocene near trench magmatism in Southern Chile: A possible manifestation of ridge collision. *Geology* 14, 23–27.

Fujiyoshi, Y., Kondo, H., Inoue, J., Yamada, T., 1987. Characteristics of precipitation and vertical structure of air temperature in Northern Patagonia. *Bulletin of Glacier Research* 4, 15–24.

Garreaud, R.D., Vuille, M., Compagnucci, R., Marengo, J., 2009. Present-day South American climate. *Palaeogeography, Palaeoclimatology, Palaeoecology* 28, 180–195.

Glasser, N.F., Harrison, S., Ivy-Ochs, S., Duller, G.A.T., Kubik, P., 2006. Evidence from the Rio Bayo valley on the extent of the North Patagonian Icefield during the Late Pleistocene–Holocene transition. *Quaternary Research* 65, 70–77.

Glasser, N.F., Harrison, S., Winchester, V., Aniya, M., 2004. Late Pleistocene and Holocene palaeoclimate and glacier fluctuations in Patagonia. *Global and Planetary Change* 43, 79–

101.

Haberle, S.G., Lumley, S.H., 1998. Age and origin of tephras recorded in postglacial lake sediments to the west of the southern Andes, 44°S to 47°S. *Journal of Volcanology nad Geothermal Research* 84, 239–256.

Haritashya, U.K., Kumar, A., Singh, P., 2010. Particle size characteristics of suspended sediment transported in meltwater from the Gangotri Glacier, central Himalaya – An indicator of subglacial sediment evacuation. *Geomorphology* 122, 140 – 152.

Harrison, S., Glasser, N.F., Duller, G.A.T., Jansson, K.N., 2012. Early and mid-Holocene age for the Tempanos moraines, Laguna San Rafael, Patagonian Chile. *Quaternary Science Reviews*, vol. 31, 82–92.

Heusser, C.J., 2002. On glaciation of the Southern Andes with special reference to the Peninsula de Taitao and adjacent Andean cordillera (~46°30'). *Journal of South American Earth Sciences* 15, 577 – 589.

Kaplan, M.R., Ackert, R.P., Singer, B.S., Douglass, D.C., Kurz, M.D., 2005. Cosmogenic nuclide chronology of millenial-scale glacial advances during O-isotope Stage 2 in Patagonia. *Bulletin of Geological Society of America* 116, 308–321.

Kissel, C., 2007. The shipboard Scientific party, MD159-PACHIDERME-IMAGES XV, cruise report. *Les rapports de campagne à la mer*. Institut Paul-Emile Victor, pp. 105.

Lamy, F., Kilian, R., Arz, H.W., François, J.P., Kaiser, J., Prange, M., Steinke, T., 2010. Holocene changes in the position and intensity of the southern westerly wind belt. *Nature Geosciences* 3, 695–699.

Lamy, F., Kaiser, J., Ninnemann, U., Hebbeln, D., Arz, H., Stoner, J., 2004. Antarctic timing of surface water changes off Chile and Patagonian Ice sheet response. *Science* 304, 1959 – 1962.

Lamy, F., Hebbeln, D., Röhl, U., Wefer, G., 2001. Holocene rainfall variability in southern Chile: a marine record of latitudinal shifts of the Southern Westerlies. *Earth and Planetary Science Letters* 185, 369–382.

Lamy, F., Hebbeln, D., Wefer, G., 1999. High resolution marine record of climate change in mid-latitude Chile during the last 28,000 years based on terrigenous sediment parameters. *Quaternary Research* 51, 83–93.

Mardones, M., González, L., King, R., Campos, E., 2011. Variaciones glaciales durante el Holoceno en Patagonia Central, Aisén, Chile: evidencias geomorfológicas. *Andean Geology* 38 (2), 371–392.

Massafero, J., Brooks, S.J., 2002. Response of chironomids to late Quaternary environmental change in the Taitao Peninsula, southern Chile. *Journal of Quaternary Science* 17, 101 – 111.

Mercer, J.H., 1982. Holocene glacier variations in Southern South America. *Striae* 18, 35–40.

Mercer, J.H., 1970. Variations of some Patagonian glaciers since the Late-Glacial, II. *American Journal of Science* 269, 1–25.

Montade, V., Combourieu Nebout, N., Chapron, E., Mulsow, S., Abarzúa, A.M., Debret, M., Foucher,

A., Desmet, M., Winiarski, T., Kissel, C., 2012. Regional vegetation and climate changes during the last 13 kyr from a marine pollen record in Seno Reloncaví, Southern Chile. *Review of Palaeobotany and Palynology* 181, 11 – 21.

Moreno, P.I., Francois, J.P., Moy, C.M., Villa-Martínez, R., 2010. Covariability of the Southern Westerlies and atmospheric CO_2 during the Holocene. *Geology* 38, 727–730.

Moreno, P.I., Jacobson, G.L., Lowell, T.V., Denton, G.H., 2001. Interhemispheric climate links revealed by a late-glacial cooling episode in southern Chile. *Nature* 409, 804–808.

Nesbitt H. W., Young G. M., 1996. Petrogenisis of sedimentsin the absence of chemical weathering: effects of abrasion and sorting on bulk composition and mineralogy. *Sedimentology* 43, 341–358.

Niemeyer, H.R., Skarmeta, J.M., Fuenzalida, R.P., Espinosa, W.N., 1984. Hojas Peninsula de Taitao y Puerto Aisen, Region Aisen del General Carlos Ibañez del Campo. *Boletin del Servicio Nacional Geologia Minera*, Carta Geologica Chile, no. 60–61, pp. 80.

Petschick, R., Kuhn, G., Gingele, F., 1996. Clay mineral distribution in surface sediments of the South Atlantic: sources, transport and relation to oceanography. *Marine Geology* 130, 203–229.

Pinchemel, P., 1952. Les terrasses marines de la Patagonie. In : *Annales de Géographie*, t.61, no. 327, pp. 378–380. Doi : 10.3406/geo.1952.13691.

Porter, S.C., 2000. Onset of Neoglaciation in the Southern Hemisphere. *Journal of Quaternary Science* 14 (4), 395–408.

Potter, P., 1994. Modern sands of South America: composition, provenance and global significance. *Geologische Rundschau* 83 (1), 212.

Putnam, A.E., Schaefer, J.M., Denton, G.H., Barrell, D.J.A., Finkel, R.C., Andersen, B.G., Schwartz, R., Chinn, T.J.H., Doughty, A.M., 2012. Regional climate control of glaciers in New Zealand and Europe during the pre-industrial Holocene. Nature Geoscience 5, 627 – 630.

Reimer, P.J., Baillie, M.G.L., Bard, E., Bayliss, A., Beck, J.W., Blackwell, P.G., Ramsey, C.B., Buck, C.E., Burr, G.S., Edwards, R.L., Friedrich, M., Grootes, P.M., Guilderson, T.P., Hajdas, I., Heaton, T.J., Hogg, A.G., Hughen, K.A., Kaiser, K.F., Kromer, B., McCormac, F.G., Manning, S.W., Reimer, R.W., Richards, D.A., Southon, J.R., Talamo, S., Turney, C.S.M., van der Plicht, J., Weyhenmeye, C.E., 2009. Intcal09 and Marine09 radiocarbon age calibration curves, 0–50,000 years cal BP. *Radiocarbon* 51, 1111–1150.

Reimer, P.J., Baillie, M.G.L., Bard, E., Bayliss, A., Beck, J.W., Bertrand, C.J.H., Blackwell, P.G., Buck, C.E., Burr, G.S., Cutler, K.B., Damon, P.E., Edwards, R.L., Fairbanks, R.G., Friedrich, M., Guilderson, T.P., Hogg, A.G., Hughen, K.A., Kromer, B., McCormac, G., Manning, S., Bronk-Ramsey, C., Reimer, R.W., Remmele, S., Southon, J.R., Stuiver, M., Talamo, S., Taylor, F.W., van der Plicht, J., Weyhenmeyer, C.E., 2004. IntCal04 terrestrial radiocarbon age calibration, 0–26 cal. kyr BP. *Radiocarbon* 46 (3), 1029–1058.

Siani, G., Michel, E., De-Pol Holt, R., Lamy, F., Carel, M., Lourantou, A., 2012. Southern Ocean deglacial reservoir age changes and timing of three episodes of upwelling. *Submitted to*

Nature Communications.

Siani G., Colin C., Michel E., Carel M., Richter T., Kissel C., Dewilde F., 2010. Late Glacial to Holocene terrigenous sediment record in the Northern Patagonian margin: Paleoclimate implications. *Palaeogeography, Palaeoclimatology, Palaeoecology* 297 (1), 26–36.

Stern, C.R., Kilian, R., 1996. Role of the subducted slab, mantle wedge and continental crust in the generation of adakites from the Andean Austral Volcanic Zone. *Contributions to Mineralogy and Petrology* 123, 263–281.

Strub P.T., Mesias J.M., Montecino V., Ruttlant J., Salinas S., 1998. Coastal ocean circulation off Western South America. In The Global Coastal Ocean. *Regional Studies and Syntheses (eds Robinson, A.R., Brink, K.H.)*, Wiley, New York. pp. 273–315.

Stuut, J-B. W., Kasten, S., Lamy, F., Hebbeln, D., 2007. Sources and modes of terrigenous sediment input to the Chilean continental slope. *Quaternary International* 161, 67–76.

Toggweiler, J.R., Russell, J.L., Carson, S.R., 2006. Midlatitude Westerlies, atmospheric CO_2, and climate change during the ice ages. *Paleoceanography*, vol. 21, PA2005, doi: 10.1029/2005PA001154.

Tonello, M. S., Mancini, M. V., Seppä, H., 2009. Quantitative reconstruction of Holocene precipitation changes in southern Patagonia. *Quaternary Research* 72, 410–420.

Varma, V., Prange, M., Lamy, F., Merkel, U., Schulz, M., 2011. Solar-forced shifts of the Southern Hemisphere Westerlies during the Holocene. *Climate of the Past* 7, 339–347.

Waldmann, N., Ariztegui, D., Anselmetti, F.S., Austin, J.A., Stern, C., Moy, C.M., Recasens, C., Dunbar, R., 2009. Holocene climatic fluctuations and positioning of the Southern Hemisphere Westerlies in Tierra del Fuego (54°S), Patagonia. *Journal of Quaternary Sciences* 25, 1063–1075.

Warren, C.R., Sugden, D.E., 1993. The Patagonian Icefields: a glaciological review. *Arctic and Alpine Research* 25 (4), 316 – 331.

Zeil, W., 1986. “Südamerika.” *Enke Verlag*, Stuttgart.

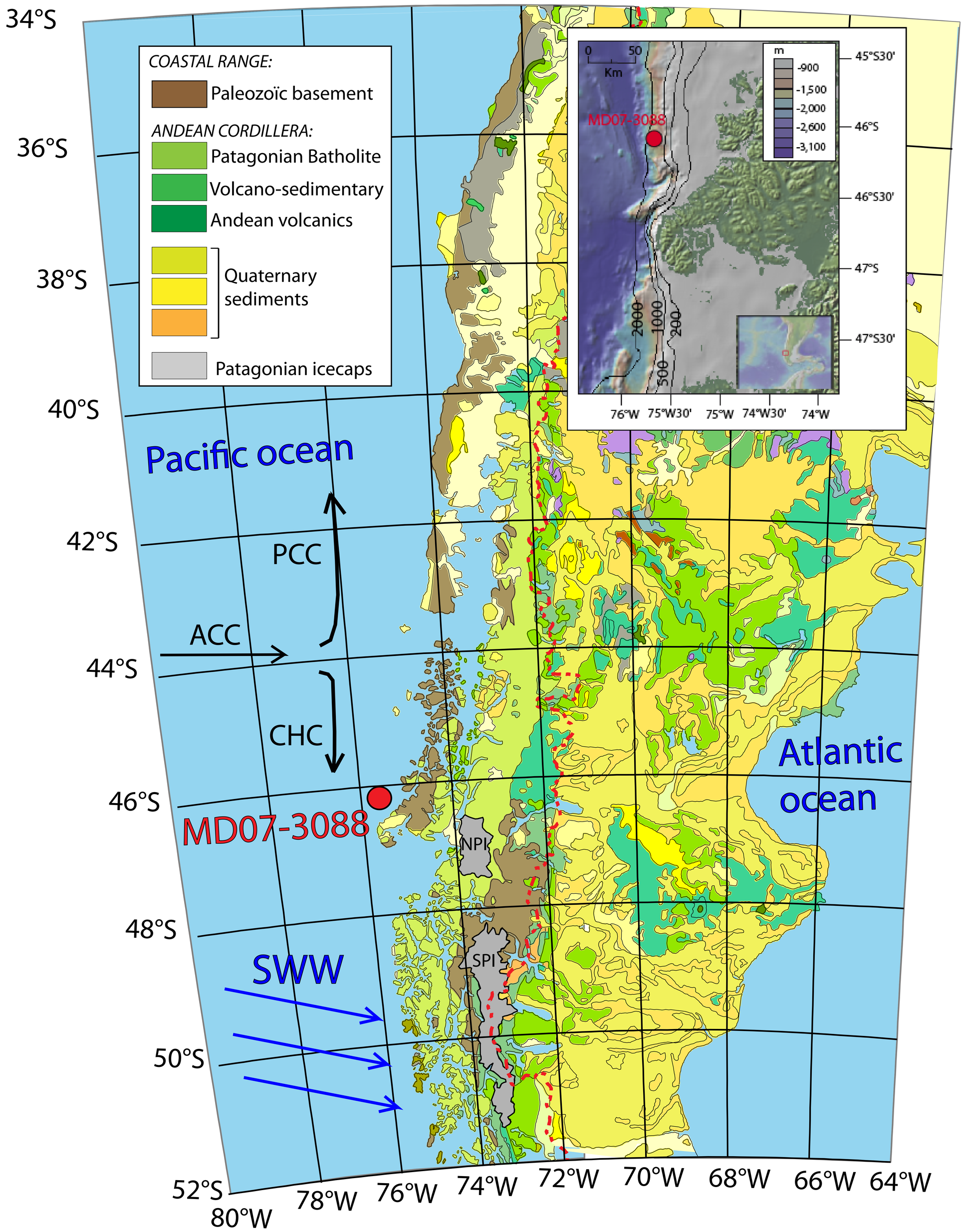

Figure 1: Southern Patagonia geological map representing the main geological units; Location of the marine record MD07-3088, repartition of the Southern Westerly winds (SWW) and distribution of shallow oceanic currents (ACC: Antarctic Circumpolar current, PCC: Peru-Chile countercurrent, CHC: Cap Horn current; Strub et al., 1998); Insert shows the bathymetry of the sampling area

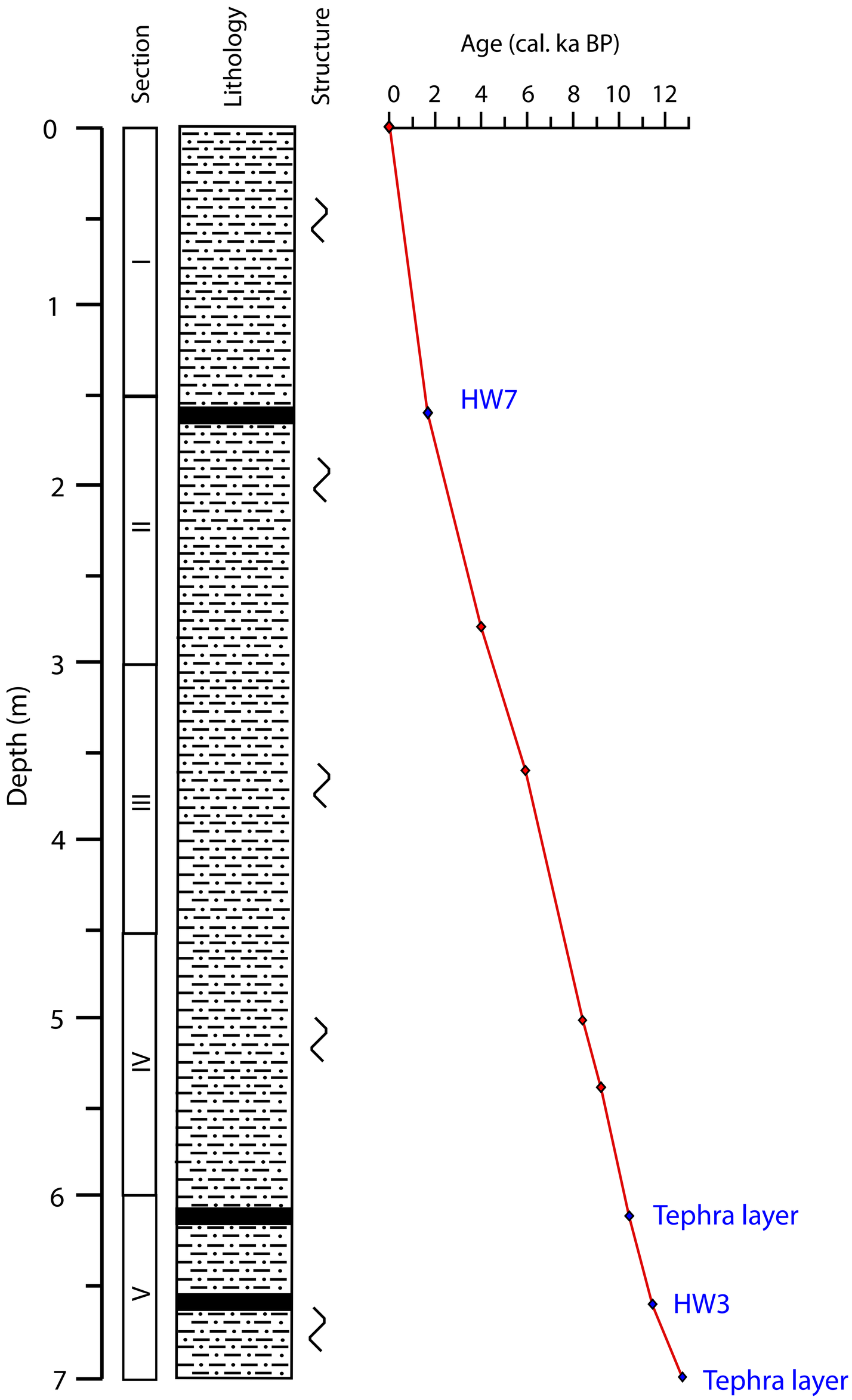

Figure 2: Lithological log of the core MD07-3088 as a function of the depth. Black lines correspond to tephra layers (1.6, 6.1 and 6.6 m) recovered in the core and correlated to well dated onland deposits (HW7 and HW3; Haberle and Lumley, 1998). Relationship between age and depth is based on 6 linearly interpolated AMS 14C dates and 3 tephra layers (Siani et al., 2010; Carel et al., 2011). 14C ages are presented in calendar ka BP according to Reimer et al., 2009.

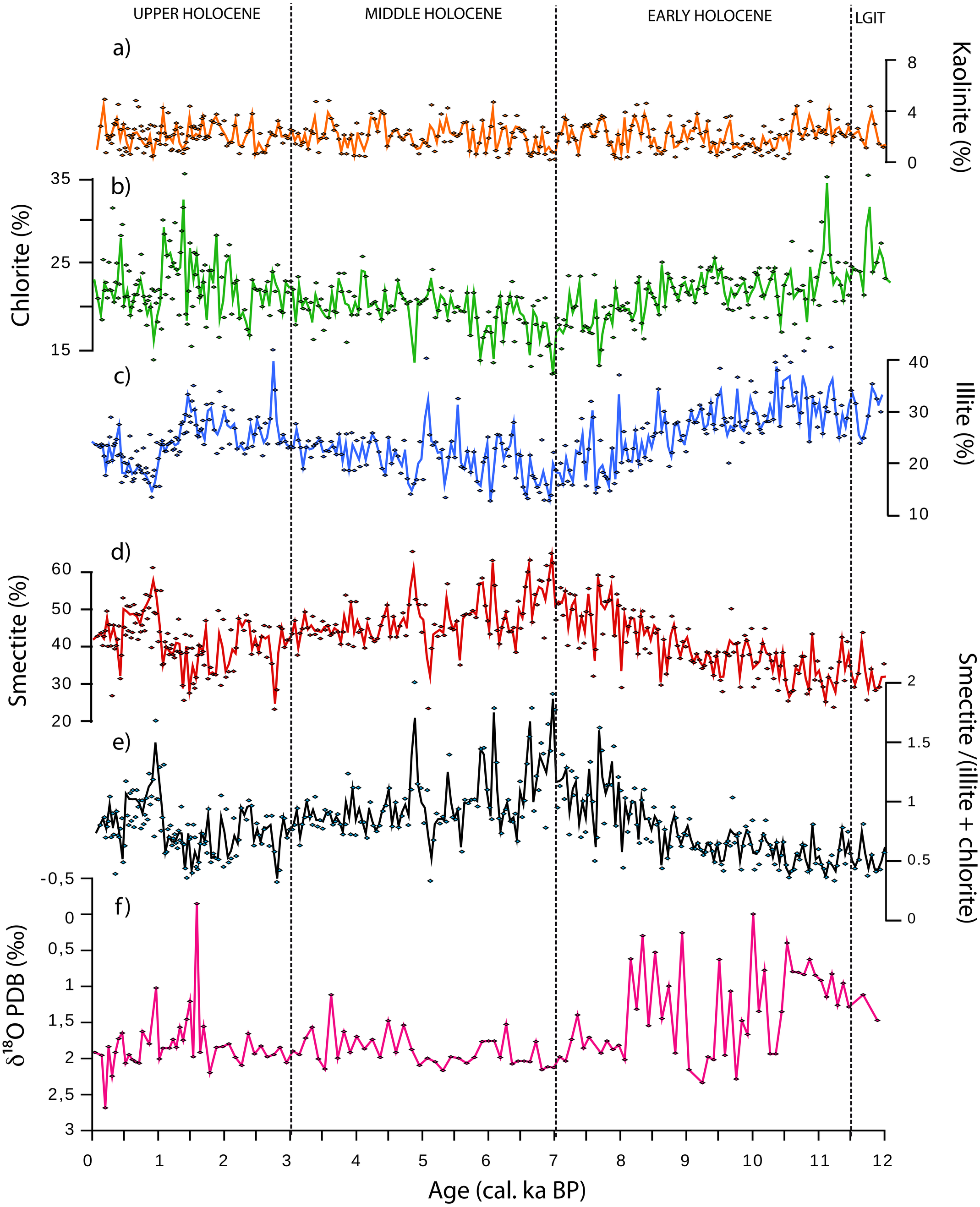

Figure 3: Distribution of the four main clay types determined by X-Ray diffraction as a function of time since the end of deglaciation (curves a,b,c and d) and the smectite/(illite+chlorite) ratio pattern (curve e) compared to the $\delta^{18}O$ signal obtained from plaktonic foraminifera shells Globigerina bulloides (curve f). Data have been fitted with a fit of 50 years.

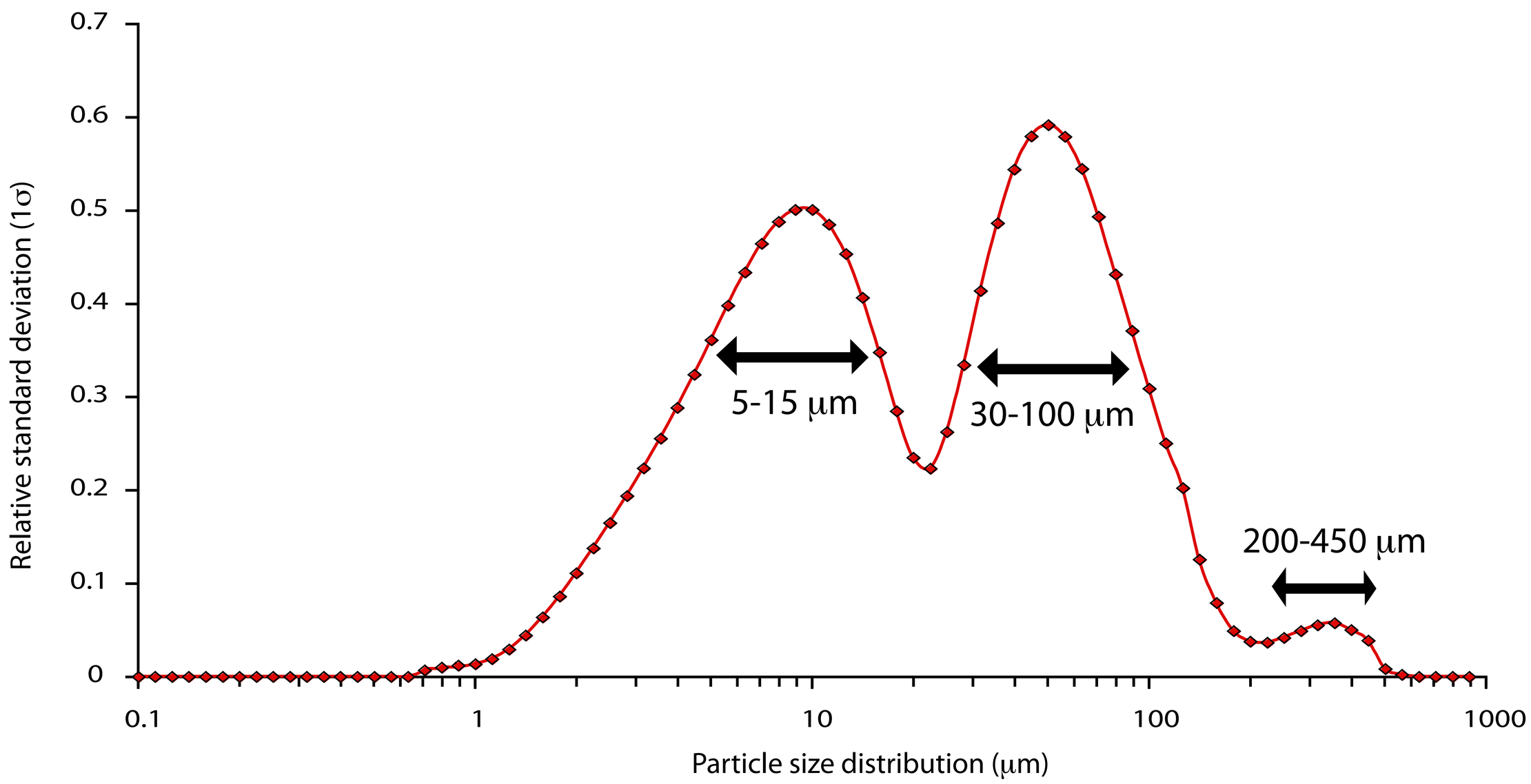

Figure 4: Distribution of the relative standard deviation as a function of particle size ranges determined by grain-size particle analyzer. Results show the dominance of three main sizes between 5-15 μm, 30-100 μm and 200-450 μm.

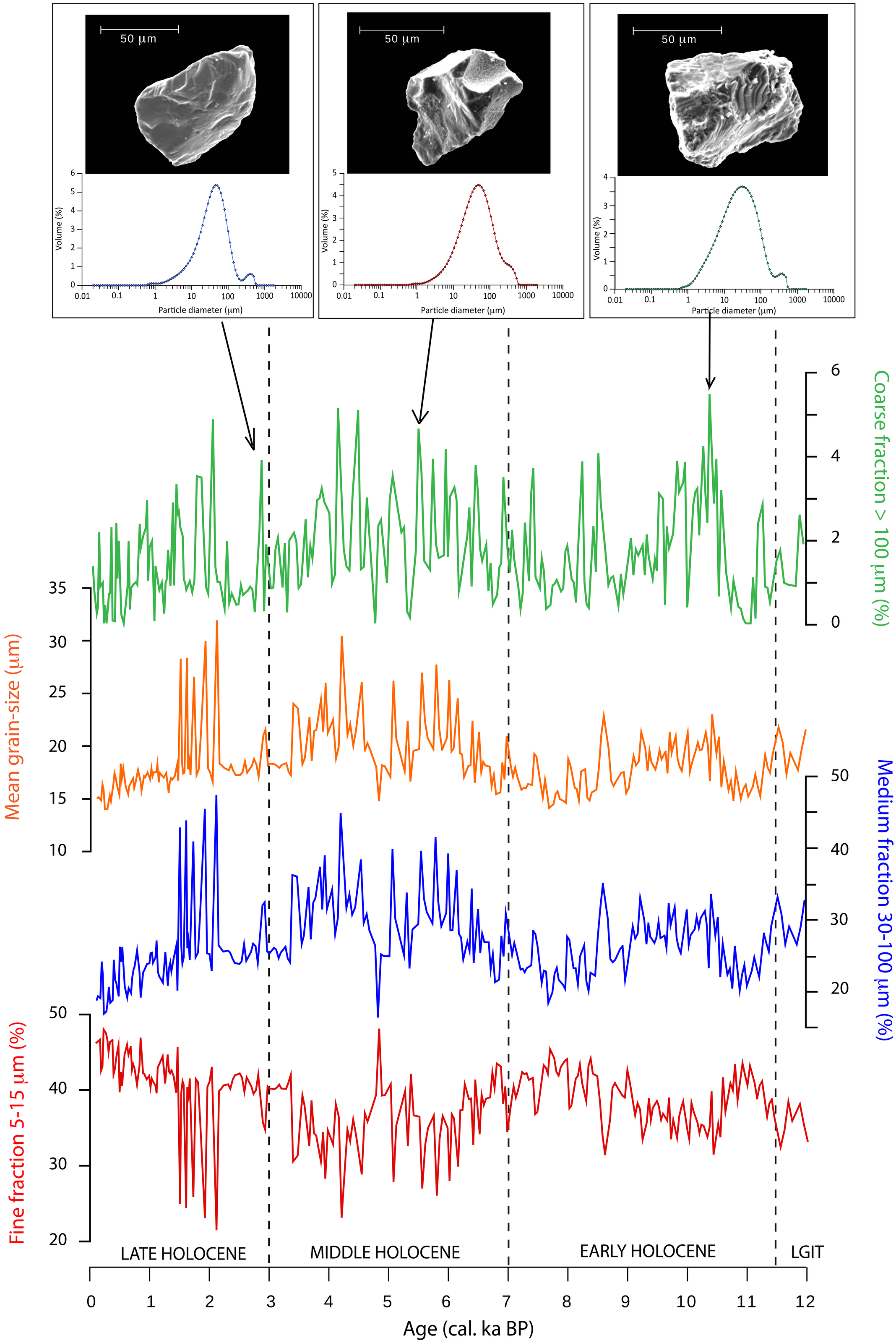

Figure 5: Grain size distribution of the fine (5-15 µm), medium (30-100 µm), the mean grain-size and coarse (>100 µm) fractions along the Holocene (the last 12 ka BP). Inserts show particles shapes obtained by SEM imaging and respective grain-size diameter of detrital particles (quartz) of three identified coarser layers

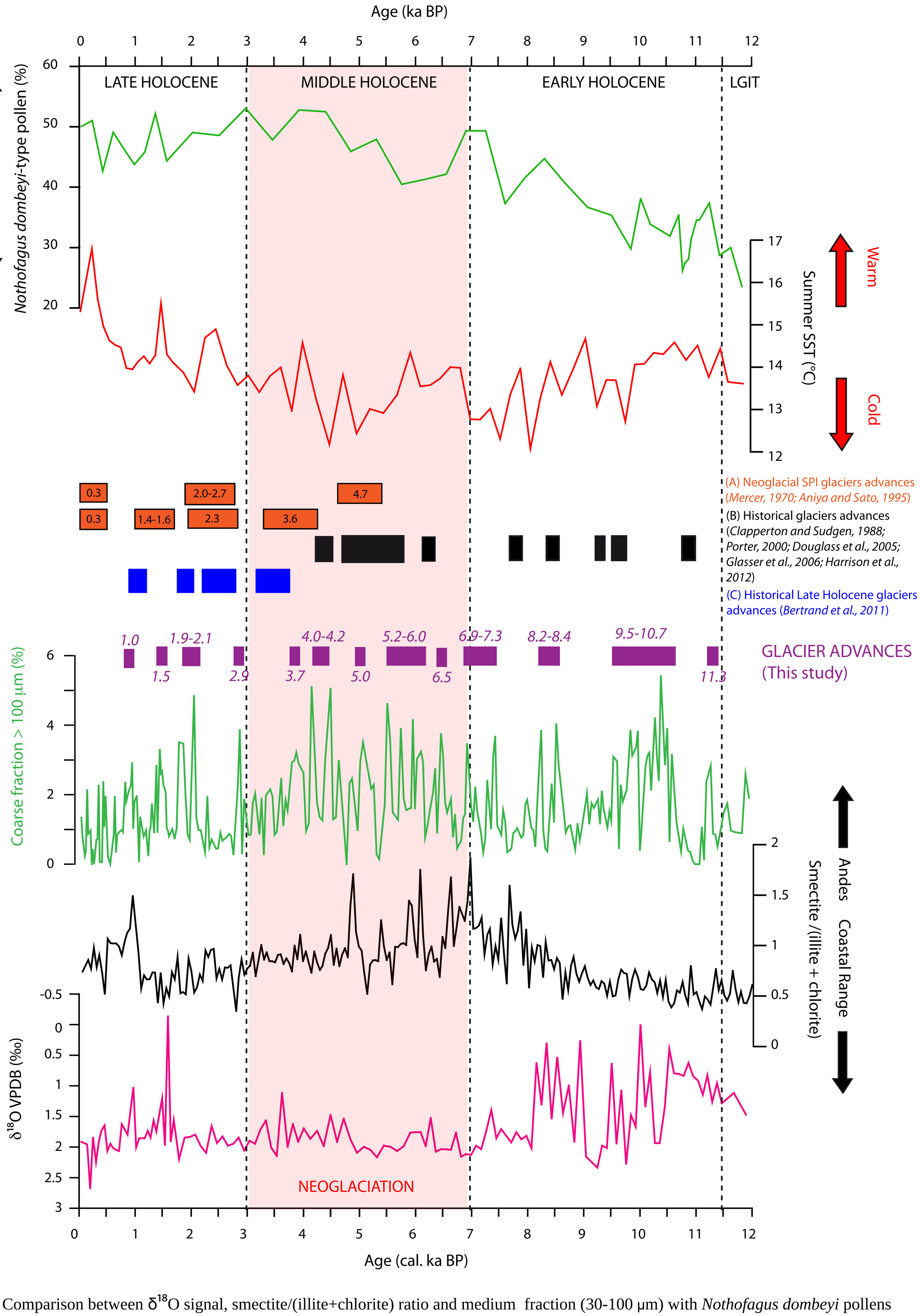

Figure 6: Comparison between $\delta^{18}O$ signal, smectite/(illite+chlorite) ratio and medium fraction (30-100 µm) with *Nothofagus dombeyi* pollens proportions, summer SST and historical glacier advance phases (coloured boxes); (A) Southern Patagonian Icecap glacier advances (Mercer, 1970 and Aniya, 1995); (B) Historical glacier advances of Southern and Northern Patagonian Icecaps determined from moraines fronts advances (Clapperton and Sudgen, 1988; Porter, 2000; Douglass et al., 2005; Glasser et al., 2006; Harrison et al., 2012); (C) Late Holocene glacial extension events (Bertrand et al., 2011) from Gualas glacier (NPI)

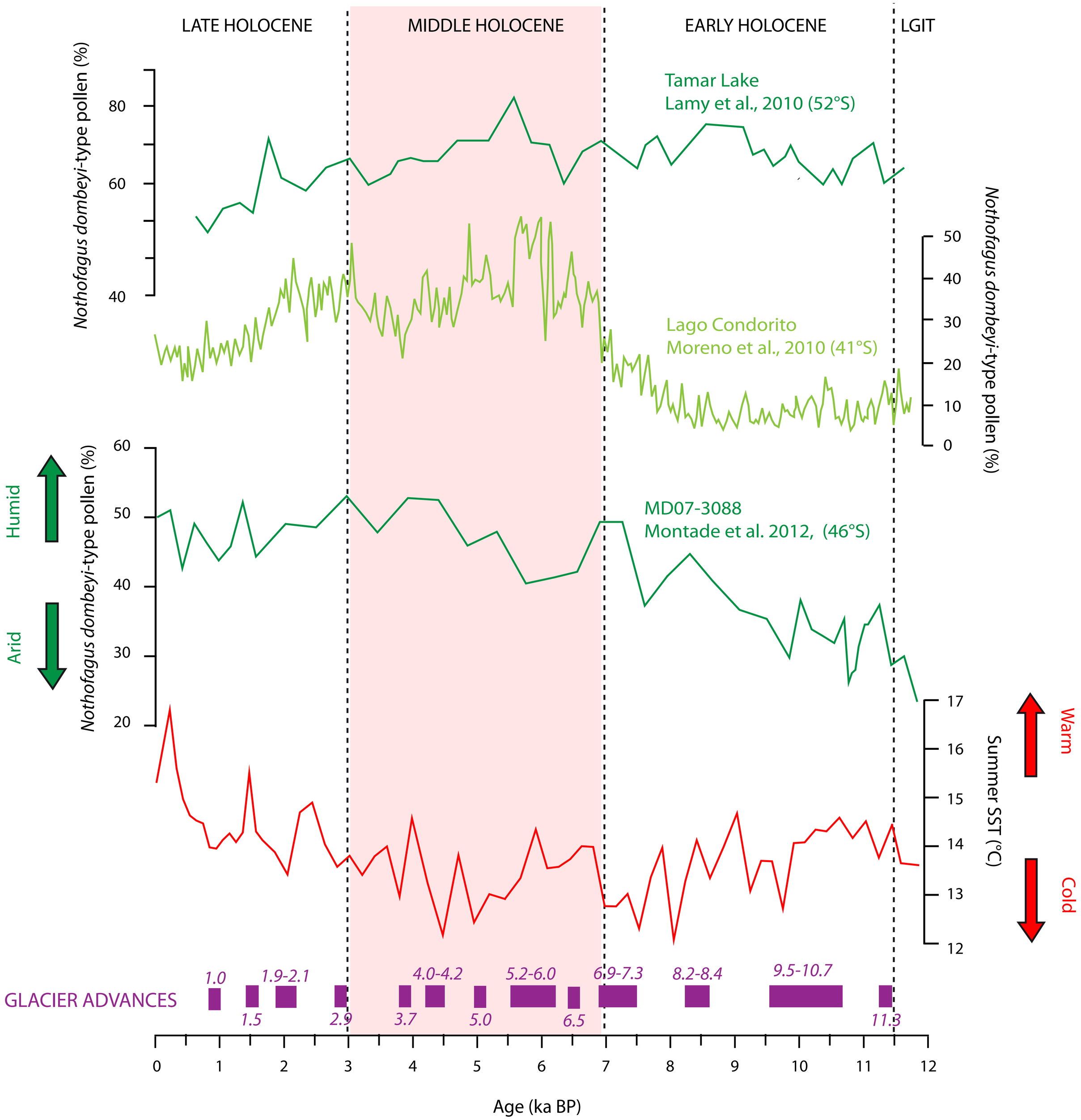

Figure 7: Comparison between glacier advances identified from grain-size, *Nothofagus-dombeyi* type pollens concentrations (%; Montade et al., 2012) and summer SST (°C) of the deep-sea core MD07-3088 (46°S) and *Nothofagus-dombeyi* type pollens concentrations (%) of two sedimentary sequences from Lago Condorito (41°S; Moreno et al., 2010) and Tamar Lake (52°S; Lamy et al., 2010)

« Late glacial to deglacial sedimentary and geochemical record from the southern chilean margin and timing of the Patagonian icefield fluctuations »
sera soumis à *Journal of Quaternary Science*

Le but principal de cet article est focalisé sur la restitution de la variabilité climatique depuis le dernier maximum glaciaire (DMG) et au cours de la Terminaison I (de 22 à 10 ka BP). Au travers des variations observées dans la minéralogie des cortèges argileux et la géochimie inorganique, il a été possible de retracer les variations dans les apports des sources continentales et l'identification de niveaux d'IRD (Ice Rafted Detritus, débris de charriage par les glaciers) a permis d'établir une nouvelle chronologie des avancées des glaciers de la calotte nord patagonienne au cours de la transition glaciaire/interglaciaire.

La mise en âge de la carotte marine MD07-3088 par un modèle d'âge bien contraint par des âges ^{14}C couplé à la stratigraphie isotopique déterminée sur les tests des foraminifères planctoniques *Globigerina bulloides*, a permis de comparer cet enregistrement avec les évènements précédemment établis par les archives climatiques continentales aux plus hautes et plus basses latitudes le long de la marge chilienne.

Les résultats ont montré que le dernier maximum glaciaire (22 à 18ka BP) est marqué par des évènements d'IRD abondants et une contribution dominante de la chaine côtière dans la source des apports détritiques. Les avancées identifiées par l'intermédiaire des traceurs climatiques sont analogues avec les estimations des phases d'expansion mises en évidence plus au sud (53°S) dont les reliques ont été observées jusqu'en Antarctique. Les températures globalement plus froides semblent contrôler les apports terrigènes et la dynamique des glaciers.

La déglaciation (18 à 11,5 ka BP) est marquée par deux épisodes majeurs de réchauffement entrecoupés par un épisode de refroidissement prononcé, l'ACR. Les deux épisodes de réchauffement marquent un changement important dans la source des apports détritiques avec une contribution plus importante des formations volcaniques de la cordillère andéenne et l'absence d'évènements de type IRD. Les conditions globalement plus chaudes résultent de la migration vers le sud de la cellule des vents dominants. En revanche, au cours de l'ACR, l'expansion des landes Magellanes, typiques d'un climat plus froid et très humide témoigne d'un déplacement vers le nord de la cellule des vents, apportant des précipitations plus intenses sur la zone d'étude et donc une accumulation de neige plus importante qui contrôle en partie la dynamique de la calotte nord patagonienne.

La récurrence d'évènements de type IRD marque un regain d'activité des glaciers de la calotte nord patagonienne.

L'intervalle terminal de la déglaciation (12.7 à 10 ka BP) est caractérisé par des conditions plus optimales induites par un retour de la cellule des vents à leur position similaire à l'actuel et une récession marquées des calottes, favorisant le démantèlement des formations volcaniques de la cordillère andéenne qui vont former la smectite.